Raman spectroscopy of graphene under ultrafast laser excitation

C. Ferrante[1*], A. Virga[1,2], L. Benfatto[3], M. Martinati[1], D. De Fazio[4], U. Sassi[4], C. Fasolato[1],

A. K. Ott[4], P. Postorino[1], D.Yoon[4], G. Cerullo[5], F. Mauri[1,2], A. C. Ferrari[4], T. Scopigno[1,2,*]

[1]*Dipartimento di Fisica, Universitá di Roma "La Sapienza", I-00185, Roma, Italy*

[2]*Istituto Italiano di Tecnologia, Center for Life Nano Science @Sapienza, Rome, Italy*

[3]*Institute for Complex Systems, CNR,*

UoS Sapienza, I-00185, Rome, Italy

[4]*Cambridge Graphene Centre, University of Cambridge, Cambridge CB3 OFA, UK*

[5]*IFN-CNR, Dipartimento di Fisica, Politecnico di Milano,*

P.zza L. da Vinci 32, 20133 Milano, Italy and

*Corresponding authors

Abstract

The equilibrium optical phonons of graphene are well characterized in terms of anharmonicity and electron-phonon interactions, however their non-equilibrium properties in the presence of hot charge carriers are still unexplored. Here we study the Raman spectrum of graphene under ultrafast laser excitation with 3ps pulses, which trade off between impulsive stimulation and spectral resolution. We localize energy into hot carriers, generating non-equilibrium temperatures in the~1700-3100K range, far exceeding that of the phonon bath, while simultaneously detecting the Raman response. The linewidth of both G and 2D peaks show an increase as function of the electronic temperature. We explain this as a result of the Dirac cones' broadening and electron-phonon scattering in the highly excited transient regime, which is critical for the emerging field of graphene-based photonics and optoelectronics.

The distribution of charge carriers has a pivotal role in determining fundamental features of condensed matter systems, such as mobility, electrical conductivity, spin-related effects, transport and optical properties. Understanding how these proprieties can be affected and, ultimately, manipulated by external perturbations is critical to technological applications in diverse areas ranging from electronics to spintronics, optoelectronics and photonics[1–3].

The current understanding of light interaction with graphene can be summarized as follows[4]. Absorbed photons create optically excited electron-hole (e-h) pairs. The subsequent relaxation towards thermal equilibrium occurs in three steps. Ultrafast electron-electron (e-e) scattering generates a hot Fermi-Dirac distribution within the first tens fs[5]. The distribution then relaxes due to scattering with optical phonons, equilibrating within 500fs[6, 7]. Finally, anharmonic decay into acoustic modes establishes thermodynamic equilibrium on the ps timescale[8–10].

Raman spectroscopy is one of the most used characterization techniques in carbon science and technology[11]. The measurement of the Raman spectrum of graphene[12] triggered a huge effort to understand phonons (ph), e-ph, magneto-ph, and e-e interactions in graphene, as well as the influence of the number and orientation of layers, electric or magnetic fields, strain, doping, disorder, quality and types of edges, and functional groups[13]. The Raman spectrum of single (SLG) and few layer graphene (FLG) consists of two fundamentally different sets of peaks. Those, such as D, G, 2D, present also in SLG, and due to in-plane vibrations[12], and others, such as the shear (C) modes[14] and the layer breathing modes[15, 16] due to relative motions of the planes themselves, either perpendicular or parallel to their normal. The G peak corresponds to the high frequency E_{2g} phonon at Γ. The D peak is due to the breathing modes of six-atom rings and requires a defect for its activation[17–19]. It comes from transverse optical (TO) phonons around the Brillouin Zone edge $\mathbf{K}$[17], it is active by double resonance (DR)[18] and it is strongly dispersive with excitation energy due to a Kohn Anomaly at $\mathbf{K}$[20]. The 2D peak is the D peak overtone. Since 2D originates from a process where momentum conservation is satisfied by two phonons with opposite wavevectors, no defects are required for its activation, and it is thus always present[12].

Raman spectroscopy is usually performed under continuous wave (CW) excitation, therefore probing samples in thermodynamic equilibrium. The fast e-e and e-ph non-radiative recombination channels establish equilibrium conditions between charge carriers and lattice,

preventing the study of the vibrational response in presence of an hot e-h population. Using an average power comparable to CW illumination (a few mW), ultrafast optical excitation can provide large fluences($\sim 1-15$J/m^2 at MHz repetition rates) over sufficiently short timescales (0.1-10ps) to impulsively generate a strongly out-of-equilibrium distributions of hot e-h pairs[4, 8, 21, 22]. Understanding the impact of the corresponding high carrier temperatures on the SLG optical phonons is an essential step for mastering out of equilibrium e-ph scattering, critical for transient photonics applications based on carrier relaxation, such as ultrafast lasers[23], detectors[1, 3] and modulators[24].

Here we characterize the optical phonons of SLG at high electronic temperatures T_e by performing Raman spectroscopy under pulsed excitation. We use a 3ps pulse to achieve a trade off between the narrow excitation bandwidth required for the necessary spectral resolution ($\frac{\delta\nu}{c}\lesssim$10cm^{-1}, being ν[Hz] the laser frequency and c the light velocity, a condition comfortably met under CW excitation) and a pulse duration, δt, sufficiently short ($\delta t \lesssim$10ps, achieved using ultrafast laser sources) to generate an highly excited carrier distribution over the equilibrium phonon population, being those two quantities Fourier conjugates[25] ($\frac{\delta\nu\cdot\delta t}{c} \geq 14.7cm^{-1}ps$). This allows us to determine the dependencies of both phonon frequency and dephasing time on the hot carriers temperature, which we explain by a broadening of the Dirac cones.

Results

Fig.1a plots a sequence of AntiStokes (AS) Raman spectra of SLG following ultrafast excitation at 1.58eV, as a function of excitation power P_L. The broad background stems from hot photoluminescence (PL) due to the inhibition of a full non-radiative recombination under high excitation densities[8, 26]. This process, absent under CW excitation in pristine SLG[27], is due to ultrafast photogeneration of charge carriers in the conduction band, congesting the e-ph decay pathway which becomes progressively less efficient with increasing fluence. This non equilibrium PL recalls the blackbody emission and can be in first approximation described by Planck's law[8]:

$$I(\hbar\omega, T_e) = \mathcal{R}(\hbar\omega)\tau_{em}\eta\frac{\hbar\omega^3}{2\pi^2c^2}\left(e^{\frac{\hbar\omega}{kT_e}} - 1\right)^{-1} \tag{1}$$
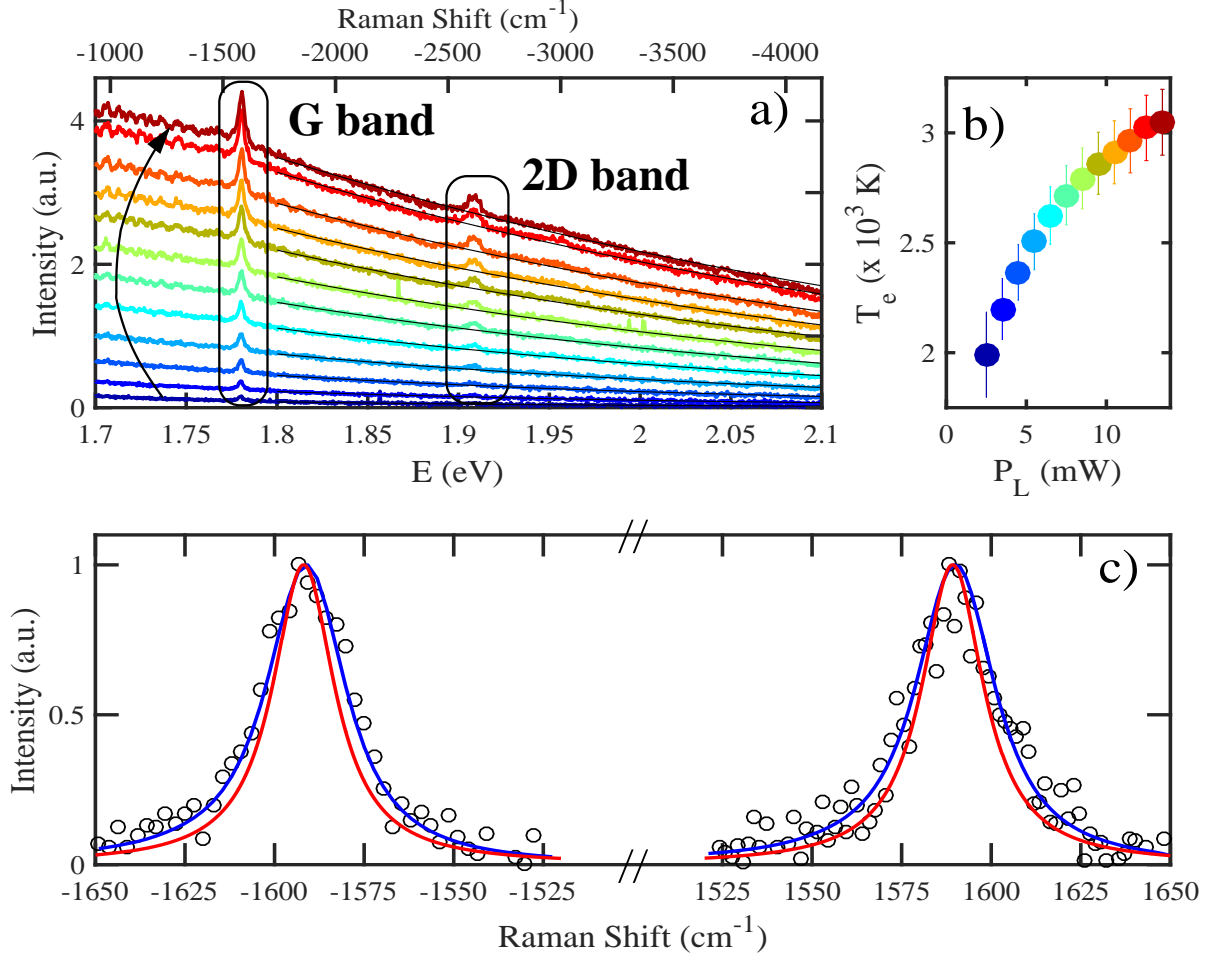
3

FIG. 1: **Spectral response of SLG.** a) AS Raman spectra under ultrafast excitation for increasing laser power, P_L, from 1.3 to 13.5mW along the arrow direction. The P_L-dependent background is fitted by thermal emission (Eq.1, black lines) resulting in T_e in the 1700-3100K range. b) T_e as a function of P_L. c) Background subtracted AS and S G peak, measured for $P_L \sim 7$mW (corresponding to $T_e \sim 2840$K). The G peak is fitted (blue line) to the experimental data (circles), as a convolution of a Lorentzian (red line) with the spectral profile of the excitation pulse.

where η is the emissivity, defined as the dimensionless ratio of the thermal radiation of the material to the radiation from an ideal black surface at the same temperature as given by the Stefan-Boltzmann law [28], τ_{em} is the emission time and $\mathcal{R}(\hbar\omega)$ is the frequency-dependent, dimensionless responsivity of our detection chain[29, 30]. By fitting the backgrounds of the Raman spectra with Eq.1 (solid lines in Fig.1a) we obtain T_e as a function of P_L. Fig.1b shows that T_e can reach up to 3100K under our pulsed excitation conditions. Assuming a full thermalization of the optical energy between vibrational and electronic degrees of
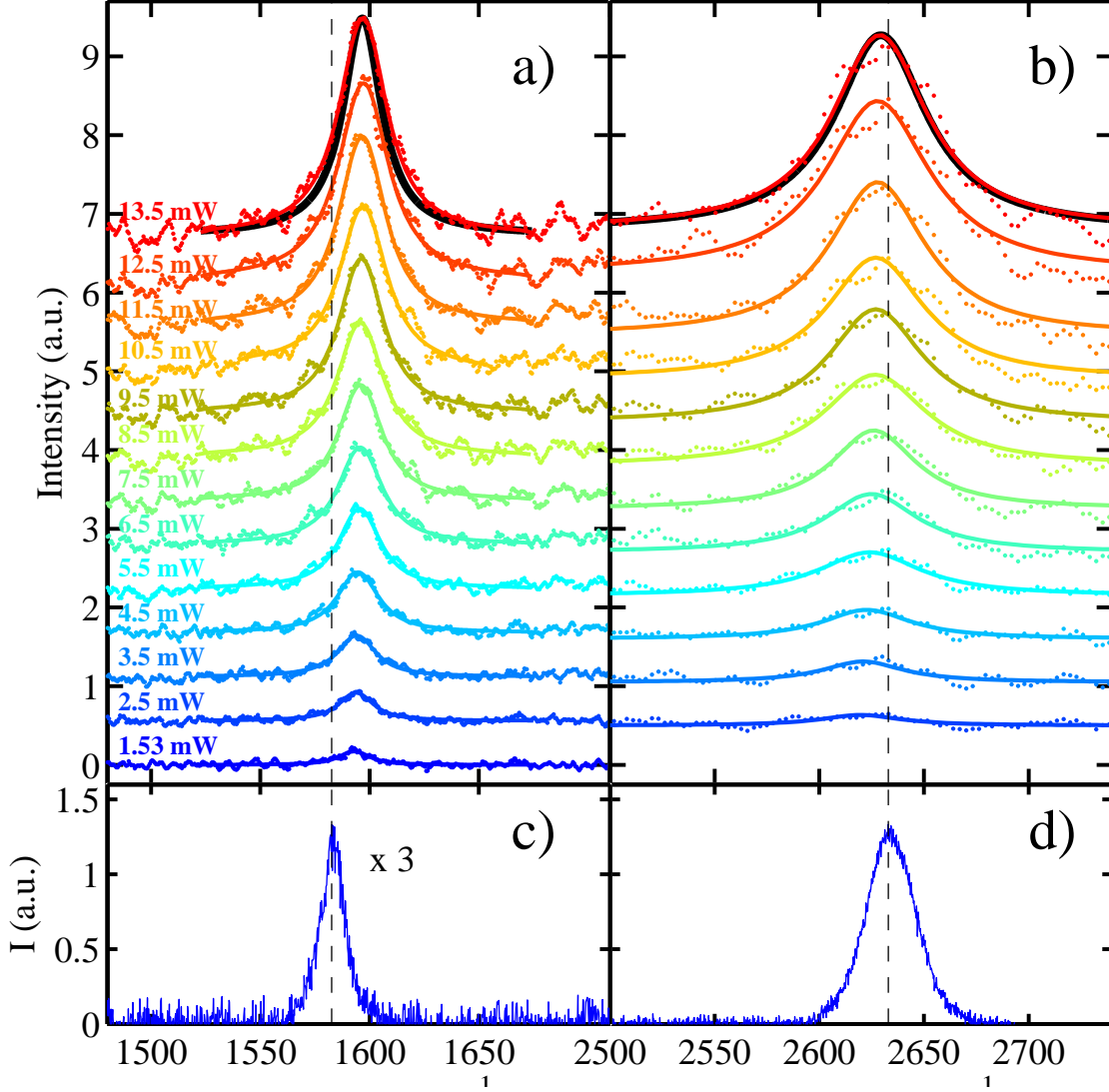
FIG. 2: (a) AS G and (b) 2D peak as function of P_L. (dots) Experimental data. (Lines) fitted Lorentzians convoluted with the spectral profile of the excitation pulse. The vertical dashed lines are the equilibrium, RT, Pos(G) and Pos(2D). (c) RT CW S G and (d) 2D peaks. The CW 2D is shifted by 5.4cm^{-1} for comparison with the AS ps-Raman, see Methods.

freedom, one can derive an estimate of the upper limit for the corresponding local equilibrium temperature, T_{eq}, see Methods. We get $T_{eq}(P_{max}) \sim 680$K at the maximum excitation power, $P_{max} = 13.5$mW. This is well below the corresponding T_e, indicating an out-of-equilibrium distribution of charge carriers. Thus, over our 3ps observation timescale, the temperature of the lattice, T_l, is well below T_{eq}.

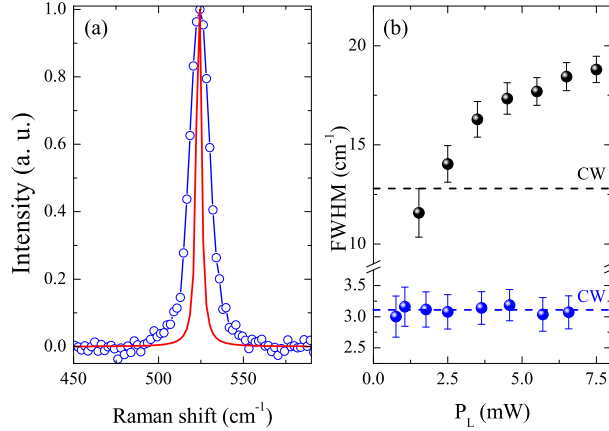Fig.1c plots the anti-Stokes (AS) and Stokes (S) G peaks, together with fits by Lorentzians

FIG. 3: **Raman response of Si for pulsed laser excitation.** (a)Raman spectrum of Si measured for ultrafast laser excitation and 6.6mW average power. (blue line) Lorentzian fit. (red line) laser-bandwidth deconvoluted spectrum. (b) FWHM(Si) as a function of P_L (blue symbols) does not show any deviation from the CW FWHM(Si) (dashed blue line). FWHM(G) under the same excitation conditions (black symbols) deviates from the CW regime (dashed black line).

(blue lines) convoluted with the laser bandwidth ($\sim 9.5 \mathrm{cm}^{-1}$), which determines the instrumental response function, IRF (see Methods). We obtain a full width at half maximum of the G peak, FWHM(G)$\sim 21 \mathrm{cm}^{-1}$, larger than the CW one ($\sim 12.7 \mathrm{cm}^{-1}$). Similarly, we obtain FWHM(2D)$\sim$50-60cm^{-1} over our P_L range, instead of FWHM(2D)$\sim 29 \mathrm{cm}^{-1}$ as measured on the same sample under CW excitation. To understand the origin of such large FWHM(G) and FWHM(2D) in pulsed excitation, we first consider the excitation power dependence of the SLG Raman response in the $1.53 - 13.5 \mathrm{mW}$ range (the lower bound is defined by the detection capability of our setup). Fig.2 plots the AS G and 2D peaks measured in the ps regime for increasing P_L, along with their Lorentzian fits. This shows that the position of the 2D peak, Pos(2D), is close to that measured under CW excitation, while the position of the G peak, Pos(G), is significantly blueshifted. Both FWHM(G) and FWHM(2D) increase with P_L. To verify that the observed peaks broadening is not limited by our IRF, we perform the same experiment on a Si substrate, Fig.3a. For this we retrieve, after deconvolution of the IRF, the same Raman linewidth measured in the CW excitation regime (Fig. 3a). The FWHM of the Si optical phonon is independent of P_L, in contrast with the well-defined dependence on P_L observed in SLG, Fig.3b.
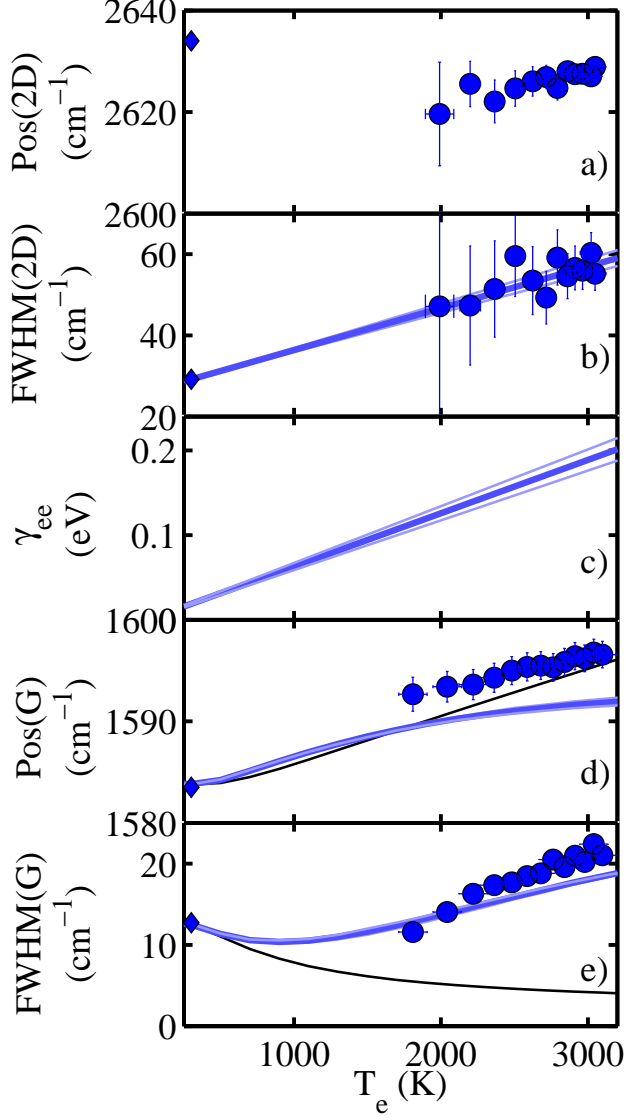
6

FIG. 4: **Comparison between theory and experiments.** a) Pos(2D), b) FWHM(2D), d) Pos(G), e) FWHM(G) as a function of T_e for ps-excited Raman spectra. Solid diamonds in a,b,d,e represent the corresponding CW measurements. FWHM(2D) are used to determine the e-e contribution (γ_{ee}) to the Dirac cones broadening, shown in (c) (blue lines). Pos(G) and FWHM(G) are compared with theoretical predictions accounting for e-ph interaction in presence of electronic broadening (an additional RT anharmonic damping$\sim$2cm^{-1}[10] is included in the calculated FWHM(G)). Black lines are the theoretical predictions for $\gamma_{ee} = 0$eV, while blue lines take into account an electronic band broadening linearly proportional to T_e ($\gamma_{ee} = \alpha_e k_B T_e$). From the fit of γ_{ee} in (c), we get $\frac{\alpha_e k_B}{hc} = 0.51$cm^{-1}/K (thickest blue line). Values of $\frac{\alpha_e k_B}{hc} = 0.46, 0.55$ cm^{-1}/K, corresponding to 99% confidence boundaries, are also shown (thin light blue lines).
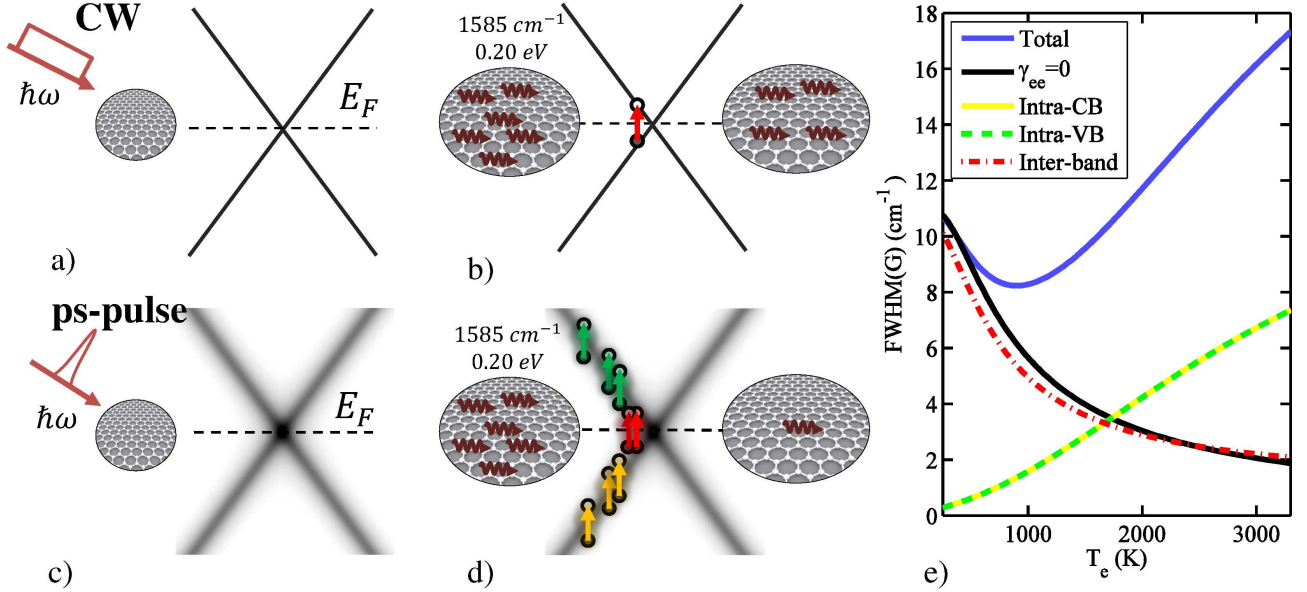
FIG. 5: **Effect of Dirac cone broadening on Raman process.** (a) CW photo-excitation with mW power does not affect the Dirac cone. (b) Accordingly, e-h formation induced by e-ph scattering only occurs in presence of resonant phonon excitation. (c) Under ps excitation, with average P_L comparable to (a), the linear dispersion is smeared by the large $k_B T_e \approx \hbar \omega_G = 0.2$eV. (d) Consequently, e-h formation is enhanced by the increased phonon absorption cross section, due to new intraband processes. (e) Corresponding contributions to FWHM(G) for the broadened inter-bands and intra-band processes for $\alpha_e k_B = 0.51$ cm^{-1}/K.

Discussion

Fig.4 plots Pos(2D), FWHM(2D), Pos(G), FWHM(G) as a function of T_e, estimated from the hot-PL. A comparison with CW measurements (633nm) at room temperature (RT) is also shown (blue diamonds). Under thermodynamic equilibrium, the temperature dependence of the Raman spectrum of SLG is dominated by anharmonicity, which is responsible for mode softening, leading to a redshift of the Raman peaks[10, 31, 32]. This differs from our experimental observation (Figs.4a-d), in which Pos(G) has an opposite trend (blue shift), and Pos(2D) is nearly T_e-independent (see Methods), indicating the absence of anharmonicity.

This suggests a dominant role of e-ph interaction on FWHM(G) and Pos(G), in the presence of a cold phonon bath at constant T_l decoupled from the (large) T_e.. To derive the temperature dependence of such parameters, we first compute the phonon self-energy

8

$\Pi(q = 0, \omega_G^0)$, as previously discussed in Refs.[20, 33, 34]:

$$\Pi(q = 0, \omega_G^0, T_e) = \xi \int_0^{\tilde{\epsilon}} d\epsilon \, \epsilon \int_{-\infty}^{+\infty} dz \, dz' \sum_{s,s'} M_s(z, \epsilon) M_{s'}(z', \epsilon) \left[\frac{f_F(z - E_F) - f_F(z' - E_F)}{z - z' - \hbar\omega_G^0 + i\delta} \right]$$
(2)

Here $\xi = g^2/(2\hbar m_a \omega_G^0 v_F^2) = 4.43 \times 10^{-3}$ is a dimensionless constant, v_F is the Fermi velocity, $\tilde{\epsilon}$ is the upper cutoff of the linear dispersion $\epsilon = v_F k$, m_a is the carbon atom mass, $\hbar\omega_G^0 = 0.196$eV the bare phonon energy, δ is a positive arbitrary small number (< 4meV), $g \sim 12.3$eV is proportional to the e-ph coupling (EPC) [6, 20, 33, 35], z, z' are the energy integration variables and $f_F(z - E_F)$ is the Fermi-Dirac distribution with E_F the Fermi energy. The two indexes $s, s' = \mp 1$ denote the e and h branches, and $M_s(z, \epsilon)$ is the corresponding spectral function, which describes the electronic dispersion.

The self-energy expressed by Eq.2 renormalizes the phonon Green's function according to the Dyson's equation[36]:

$$D(\omega) = \frac{2\hbar\omega_G^0}{(\hbar\omega + i\delta)^2 - (\hbar\omega_G^0)^2 - 2\hbar\omega_G^0 \Pi(\omega)}$$
(3)

so that the shift $\Delta\text{Pos(G)}$ and FWHM(G) can be written as:

$$\Delta\text{POS(G)} = \frac{1}{hc}\text{Re}\left[\Pi(0, \omega_G^0, T_e) - \Pi(0, \omega_G^0, T_e = 0)\right]$$
$$\text{FWHM(G)} = -\frac{2}{hc}\text{Im}\Pi(0, \omega_G^0, T_e)$$
(4)

where h is the Planck constant. FWHM(G) can be further simplified since the evaluation of $\text{Im}\Pi(0, \omega_G^0, T_e)$ leads to $\delta(z - z' - \hbar\omega_G^0)$ in Eq.2, so that we get:

$$\text{FWHM(G)} = \frac{\pi\xi}{hc} \int_0^{\tilde{\epsilon}} d\epsilon \, \epsilon \int_{-\infty}^{+\infty} dz \sum_{s,s'} M_s(z, \epsilon) M_{s'}(z - \hbar\omega_G^0, \epsilon) \left[f_F(z - E_F) - f_F(z - \hbar\omega_G^0 - E_F)\right]$$
(5)

In the limit of vanishing broadening of the quasiparticle state, the SLG gapless linear dispersion is represented by the following spectral function[36]:

$$M_s(z, \epsilon) = \delta(z + s\epsilon), \quad s = \pm 1,$$
(6)

This rules the energy conservation in Eq.5 and allows only transitions between h and e states with energy difference $2\epsilon = \hbar\omega_G^0$. Thus, we get[20, 33, 34]:

$$\text{FWHM(G)} = = \text{FWHM(G)}^0 \left[f_F(-\hbar\omega_G^0/2 - E_F) - f_F(\hbar\omega_G^0/2 - E_F)\right]$$
(7)

9

where $\mathrm{FWHM(G)}^0 = \frac{\pi\xi\hbar\omega_G^0}{2hc} \sim 11\mathrm{cm}^{-1}$[10]. This value, with the additional $\sim 2\mathrm{cm}^{-1}$ contribution arising from anharmonic effects[10], is in agreement with the CW measurement at $T_e = T_{eq} = 300\mathrm{K}$ (see diamond in Fig.4e) corresponding to fluences $\ll 1\mathrm{J/m}^2$. Eq.7 also shows that, as T_e increases, the conduction band becomes increasingly populated, making progressively less efficient the phonon decay channel related to e-h formation and leading to an increase of the phonon decay time (Fig.5b). This leads to a decrease of FWHM(G) for increasing T_e (black solid line in Fig.4e), which is in contrast with the experimentally observed increase (blue circles in Fig.4e).

A more realistic description may be obtained by accounting for the effect of T_e on the energy broadening (γ_e) of the linear dispersion $M_s(z,\epsilon)$, along with the smearing of the Fermi function. $\gamma_e(z, T_e)$ can be expressed, to a first approximation, as the sum of three terms[37]:

$$\gamma_e(z, T_e) = \gamma_{ee}(T_e) + \gamma_{ep}(z) + \gamma_{def}(z) \tag{8}$$

where γ_{ee}, γ_{ep} and γ_{def} are the e-e, e-ph and defect contributions to γ_e. The only term that significantly depends on T_e is γ_{ee}, while the others depend on the energy z[10, 34, 37–40].

The linear dependence of γ_{ee} on T_e [41] can be estimated from its impact on FWHM(2D). The variation of FWHM(2D) with respect to the RT value can be written as[32]:

$$\Delta\mathrm{FWHM(2D)} = 4\sqrt{2^{2/3}-1}\frac{1}{2}\frac{\partial\mathrm{POS(2D)}}{\partial(h\nu_{laser})}\gamma_{ee} \tag{9}$$

where $[\partial\mathrm{POS(2D)}/\partial(h\nu_{laser})]/2 = \frac{1}{ch}v_{ph}/v_F \sim 100\mathrm{cm}^{-1}/\mathrm{eV}$ [13, 42], i.e. the ratio between the phonon and Fermi velocity, defined as the slope of the phononic (electronic) dispersion at the ph (e) momentum corresponding to a given excitation laser energy $h\nu_{laser}$[13]. Since the DR process responsible for the 2D peak involves the creation of e-h pairs at energy $\mp h\nu_{laser}/2$, the variation of FWHM(2D) allows us to estimate the variation of γ_e at $z = h\nu_{laser}/2 \simeq 0.8\mathrm{eV}$. Then, γ_{ep} and γ_{def}, both proportional to z ($\gamma_{ep}, \gamma_{def} \propto z$), will give an additional constant contribution to FWHM(2D), but not to its variation with T_e. Our data support the predicted[41] linear increase of γ_{ee} with T_e, with an dimensionless experimental slope $\alpha_e \simeq 0.73$, Fig.4c.

In order to compute FWHM(G) from Eq.2, we note that the terms γ_{ep} and γ_{def} are negligible at the relevant low energy $z = \hbar\omega_G/2 \sim 0.1\mathrm{eV} \ll h\nu_{laser}/2$. Hence $\gamma_e(z, T_e) \simeq \gamma_{ee}(T_e)$.

The Dirac cone broadening can now be introduced by accounting for γ_e in the spectral function of Eq.6:

$$M_s(z) = \frac{1}{\pi} \frac{\gamma_e/2}{(z + s\epsilon)^2 + (\gamma_e/2)^2}, \quad s = \pm 1, \tag{10}$$

accordingly, *all* the processes where the energy difference $|s\epsilon(k) - s'\epsilon(k') + \hbar\omega_0|$ is less than $2\gamma_e$ (which guarantees the overlap between the spectral functions of the quasiparticles) will now contribute in Eq.2. Amongst them, those transitions within the same (valence or conduction) band, as shown in Fig.5d.

The broadened interband contributions still follow, approximately, Eq.7 (see Fig.5e). However, the Dirac cone broadening makes additional channels for G phonon annihilation by carrier excitation available. In particular, intra-band transitions within the Dirac cone are now progressively enabled for increasing T_e, as sketched in Fig 5d. In Fig.5e the corresponding contributions to the linewidth of the G mode are shown.

Critically, the new intraband processes produce an increasing FWHM(G), which becomes dominant beyond $T_e \sim 1000$K. As a consequence, the overall efficiency of the e-ph channel increases, producing, in turn, a dephasing time reduction, corresponding to the experimentally observed FWHM(G) increase.

Calculations in the weak-coupling limit[41] suggest that $\gamma_e(T_e)$ should be suppressed as $z \to 0$, due to phase-space restriction of the Dirac-cone dispersion. Our results, however, indicate that this effect should appear at an energy scale smaller than $\hbar\omega_G/2$, as the theory captures the main experimental trends, just based on a z-independent $\gamma_e(T_e)$.

In conclusion, we measured the Raman spectrum of SLG with impulsive excitation, in the presence of a distribution of hot charge carriers. The chosen excitation bandwidth enables us to combine frequency resolution, required to observe the Raman spectra, with short pulse duration, needed to create a significant population of hot carriers not equilibrated with the lattice. We show that, under these strongly non-equilibrium conditions, the Raman spectrum of graphene cannot be understood based on the standard low fluence picture, and we provide the experimental demonstration of a broadening of the electronic linear dispersion induced by the highly excited carriers. Our results shed light on a novel regime of non-equilibrium Raman response of SLG, whereby the e-ph interaction is enhanced. In view of the consequent implications for the transient charge carrier mobility under photoexcitation, we anticipate these findings to be crucial for the understanding and the modeling of SLG-based optoelectronic and photonic devices[43, 44].

Methods

Sample preparation and CW Raman characterization

SLG is grown on a 35μm Cu foil, following the process described in Refs.45,46. The substrate is heated to 1000°C and annealed in hydrogen (H_2, 20 sccm) for 30 minutes. Then, 5 sccm of methane (CH_4) is let into the chamber for the following 30 minutes so that the growth can take place[45, 46]. The sample is then cooled back to RT in vacuum ($\sim$1 mTorr) and unloaded from the chamber. The sample is characterized by CW Raman spectroscopy using a Renishaw inVia Spectrometer equipped with a 100x objective. The Raman spectrum measured at 514 nm is shown in Fig.6 (red curve). This is obtained by removing the non-flat background Cu PL[47]. The absence of a significant D peak implies negligible defects[12, 13, 19, 48]. The 2D peak is a single sharp Lorentzian with FWHM(2D)$\sim$23cm^{-1}, a signature of SLG[12]. Pos(G) is$\sim$1587cm^{-1}, with FWHM(G)$\sim$14cm^{-1}. Pos(2D) is$\sim$2705cm^{-1}, while the 2D to G peak area ratio is $\sim$4.3, indicating a p-doping$\sim$250meV[40, 49, 50], which corresponds to a carrier concentration$\sim$4$\cdot$10^{12}cm^{-2}. SLG is then transferred on glass by a wet method[51]. Poly-methyl methacrylate (PMMA) is spin coated on the substrate, which is then placed in a solution of ammonium persulfate (APS) and deionized water. Cu is etched[45, 51], the PMMA membrane with attached SLG is then moved to a beaker with deionized water to remove APS residuals. The membrane is subsequently lifted with the target substrate. After drying, PMMA is removed in acetone leaving SLG on glass. The SLG quality is also monitored after transfer. The Raman spectrum of the substrate shows features in the D and G peak range, convoluted with the spectrum of SLG on glass (blue curve in Fig.6). A point-to-point subtraction is needed to reveal the SLG features. After transfer, the D peak is still negligible, demonstrating that no significant additional defects are induced by the transfer process.

Before and after the pulsed laser experiment, equilibrium CW measurements are performed at room temperature using a micro-Raman setup (LabRAM Infinity), as shown in Figs.2,4. Pos(G), FWHM(G), Pos(2D) and FWHM(2D) are extracted from the S side, as the AS is much weaker due to the detailed balance condition. A different energy and momentum of the D phonon is involved, for a given excitation wavelength, in the S or AS processes, due to the phonon dispersion in the DR mechanism[52, 53]. Hence, in order to measure
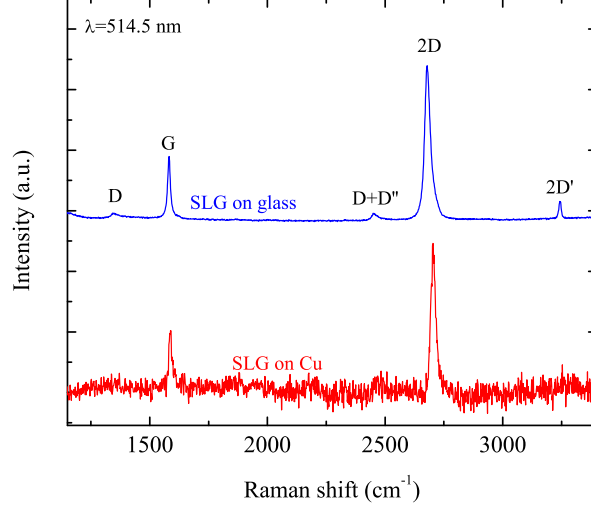
FIG. 6: **CW Raman spectra of SLG.** Raman response of SLG on Cu (red line), and on glass (blue line) after the transfer from Cu substrate. In the latter case, the substrate spectrum is subtracted.

the same D phonon in S and AS, different laser excitations (ν_{laser}) must be used according to $\nu_{laser}^S = \nu_{laser}^{AS} + c\text{Pos}(2D)$[13, 54, 55]. Given our pulsed laser wavelength (783nm), the corresponding CW excitation would be~649.5nm. Hence, we use a 632.8nm He-Ne source, accounting for the small residual wavelength mismatch by scaling the phonon frequency as $\frac{d\text{Pos}(2D)}{d\nu_{laser}} = 0.0132/c$[13]

Pulsed Raman measurements

The ps-Raman apparatus, developed at the Femtoscopy labs ("Sapienza"University of Rome), is based on a mode-locked Er:fiber amplified laser at~ 1550nm, producing 90fs pulses at a repetition rate RR=40MHz. Using second-harmonic generation in a 1cm Periodically Poled Lithium Niobate crystal[56], we obtain 3ps pulses at 783nm with a~ 9.5cm^{-1} bandwidth. The beam is focused on SLG through a slightly underfilled 20X objective (NA= 0.4), resulting in a focal diameter $D = 5.7\mu$m. Back-scattered light is collected by the same objective, separated with a dichroic filter from the incident beam and sent to a spectrometer, whose resolution can be adjusted by adopting two gratings (0.13nm or 0.028nm per pixel). The overall IRF, however, is dominated by the additional contribution induced by the finite excitation pulse bandwidth. Hence, in order to extract the FWHM of the Raman peaks, our

data are fitted convolving a Lorentzian with the spectral profile of the laser excitation. The S signal in Fig.1c is obtained as the difference spectrum of two measurements with excitation frequencies slightly offset by$\sim$130cm^{-1}, resulting in PL suppression.

Estimate of the local equilibrium temperature T_{eq}

Photoexcitation of SLG induces an excess of energy in the form of heat Q per unit area, that can be expressed as:

$$Q \sim \frac{P_L}{RR} \frac{A}{\pi W^2} \qquad (11)$$

where $A = 2.3\%$ is the SLG absorption, approximated to the undoped case[57], $W \sim 2.8\mu$m is the waist of focused beam and $RR = 40$MHz is the repetition rate of the excitation laser. The induced T_{eq} can be derived based on two assumptions: (i) in our ps time scale the energy absorbed in the focal region does not diffuse laterally, (ii) the energy is equally distributed on each degree of freedom (electrons, optical and acoustic ph). Then, Q can be described as:

$$Q = \int_{RT}^{T_{eq}} C(T) \, dT \qquad (12)$$

where $C(T)$ is the SLG T-dependent specific heat. In the $300 - 700$K range, $C(T)$ can be described as[58]: $C(T) = aT + b$, where $a = 1.35 \cdot 10^{-6}$J/(K$^2 \cdot$m^2) and $b = 1.35 \cdot 10^{-4}$J/(K$\cdot$m^2). Therefore, considering Eqs.11,12, for $P_L = P^{max} = 13.5$mW, we get $T_{eq} \sim 680$K, well below the corresponding T_e, indicating an out-of-equilibrium condition ($T_l < T_{eq} < T_e$).

Estimate of Pos(2D) as a function of T_e

We perform calculations within the Local Density Approximation, using the density functional perturbation theory (DFPT)[59, 60]. We use the experimental lattice parameter 2.46Å[61] and plane waves (45Ry cutoff), within a norm-conserving pseudopotential approach[60]. The electronic levels are occupied with a finite fictitious T_e with a Fermi Dirac distribution, and we sample a Brillouin Zone with a 160x160x1 mesh. This does not take into account anharmonic effects, assuming $T_l = 300$K. Fig.7 shows a weak $\Delta Pos(2D)(\sim 5$cm$^{-1})$ in the range $T_e = 300 - 3000$K. In equilibrium, $T_l = T_e$ would induce a non-negligible anharmonicity[62], which would lead to a Pos(2D) softening: $\Delta Pos(2D)/\Delta T_{eq} = -0.05$ cm^{-1}/K. The weak dependence $\Delta Pos(2D)(P_L)$ (blue circles in Fig.7) rules out a dominant
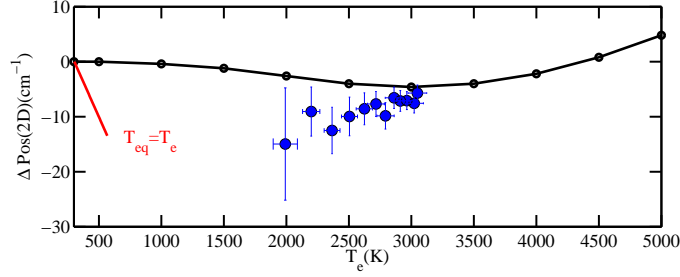
FIG. 7: **Temperature dependence of Pos(2D).** Pos(2D), relative to the RT CW measurement, as a function of T_e. Black line: DFPT calculation; Blue circles: experimental data with pulsed excitation. Red line: T-dependent CW measurement in thermal equilibrium ($T_e = T_l = T_{eq}$) from Ref.[62].

anharmonicity contribution and, consequently, $T_l = T_e$. The minor disagreement with DFPT suggests a T_l slightly larger than RT, but definitely smaller than T_{eq}.

Acknowledgments

———————

[1] F. Bonaccorso, Z. Sun, T. Hasan, and A. C. Ferrari, Nat. Photon. **4**, 611 (2010).

[2] A. C. Ferrari, F. Bonaccorso, V. Fal'ko, K. S. Novoselov, S. Roche, P. Boggild, S. Borini, F. H. L. Koppens, V. Palermo, N. Pugno, et al., Nanoscale **7**, 4598 (2015).

[3] F. H. L. Koppens, T. Mueller, T. Hasan, P. Avouris, A. C. Ferrari, M. S. Vitiello, and M. Polini, Nat. Nanotech. **9**, 780 (2014).

[4] D. Brida, A. Tomadin, C. Manzoni, Y. J. Kim, A. Lombardo, S. Milana, R. R. Nair, K. S. Novoselov, A. C. Ferrari, G. Cerullo, et al., Nat. Commun. **4** (2013).

[5] A. Tomadin, D. Brida, G. Cerullo, A. C. Ferrari, and M. Polini, Phys. Rev. B **88**, 035430 (2013).

[6] M. Lazzeri, S. Piscanec, F. Mauri, A. C. Ferrari, and J. Robertson, Phys. Rev. Lett. **95**, 236802 (2005).

[7] S. Butscher, F. Milde, M. Hirtschulz, E. Malič, and A. Knorr, Appl. Phys. Lett. **91**, 203103 (2007).

[8] C. H. Lui, K. F. Mak, J. Shan, and T. F. Heinz, Phys. Rev. Lett. **105**, 127404 (2010).

[9] S. Wu, W.-T. Liu, X. Liang, P. J. Schuck, F. Wang, Y. R. Shen, and M. Salmeron, Nano Lett. **12**, 5495 (2012).

[10] N. Bonini, M. Lazzeri, N. Marzari, and F. Mauri, Phys. Rev. Lett. **99**, 176802 (2007).

[11] A. C. Ferrari and J. e. Robertson, Phil. Trans. R. Soc. Lond. A **362**, 2267 (2004).

[12] A. C. Ferrari, J. C. Meyer, V. Scardaci, C. Casiraghi, M. Lazzeri, F. Mauri, S. Piscanec, D. Jiang, K. S. Novoselov, S. Roth, et al., Phys. Rev. Lett. **97**, 187401 (2006).

[13] A. C. Ferrari and D. M. Basko, Nat. Nanotech. **8**, 235 (2013).

[14] P. H. Tan, W. P. Han, W. J. Zhao, Z. H. Wu, K. Chang, H. Wang, Y. F. Wang, N. Bonini, N. Marzari, N. Pugno, et al., Nat. Mater. **11**, 294 (2012).

[15] K. Sato, J. S. Park, R. Saito, C. Cong, T. Yu, C. H. Lui, T. F. Heinz, G. Dresselhaus, and M. S. Dresselhaus, Phys. Rev. B **84**, 035419 (2011).

[16] C. H. Lui, L. M. Malard, S. Kim, G. Lantz, F. E. Laverge, R. Saito, and T. F. Heinz, Nano Lett. **12**, 5539 (2012).

[17] F. Tuinstra and J. L. Koenig, J. Chem. Phys. **53**, 1126 (1970).

[18] C. Thomsen and S. Reich, Phys. Rev. Lett. **85**, 5214 (2000).

[19] A. C. Ferrari and J. Robertson, Phys. Rev. B **61**, 14095 (2000).

[20] S. Piscanec, M. Lazzeri, F. Mauri, A. C. Ferrari, and J. Robertson, Phys. Rev. Lett. **93**, 185503 (2004).

[21] H. Yan, D. Song, K. F. Mak, I. Chatzakis, J. Maultzsch, and T. F. Heinz, Phys. Rev. B **80**, 121403 (2009).

[22] M. Breusing, S. Kuehn, T. Winzer, E. Malič, F. Milde, N. Severin, J. P. Rabe, C. Ropers, A. Knorr, and T. Elsaesser, Phys. Rev. B **83**, 153410 (2011).

[23] Z. Sun, T. Hasan, F. Torrisi, D. Popa, G. Privitera, F. Wang, F. Bonaccorso, D. M. Basko, and A. C. Ferrari, ACS Nano **4**, 803 (2010).

[24] M. Liu, X. Yin, E. Ulin-Avila, B. Geng, T. Zentgraf, L. Ju, F. Wang, and X. Zhang, Nature **474**, 64 (2011).

[25] A. Papoulis, *The Fourier Integral and Its Applications* (Mcgraw-Hill College, New York, 1962), first edition edition ed.

[26] R. J. Stöhr, R. Kolesov, J. Pflaum, and J. Wrachtrup, Phys. Rev. B **82**, 121408 (2010).

[27] T. Gokus, R. R. Nair, A. Bonetti, M. Bhmler, A. Lombardo, K. S. Novoselov, A. K. Geim, A. C. Ferrari, and A. Hartschuh, ACS Nano **3**, 3963 (2009).

[28] H. B. Callen, *Thermodynamics and an Introduction to Thermostatistics* (John Wiley & Sons Inc, New York, 1985).

[29] URL `http://www.princetoninstruments.com/calculators/grating-dispersion.cfm`.

[30] URL `http://www.princetoninstruments.com/userfiles/files/assetLibrary/Datasheets/Princeton_`

[31] A. T. Apostolov, I. N. Apostolova, and J. M. Wesselinowa, J. Phys. Condens. Matter **24**, 235401 (2012).

[32] D. M. Basko, Phys. Rev. B **78**, 125418 (2008).

[33] M. Lazzeri and F. Mauri, Phys. Rev. Lett. **97**, 266407 (2006).

[34] S. Pisana, M. Lazzeri, C. Casiraghi, K. S. Novoselov, A. K. Geim, A. C. Ferrari, and F. Mauri, Nat. Mater. **6**, 198 (2007).

[35] A. C. Ferrari, Solid State Commun. **143**, 47 (2007), exploring grapheneRecent research advances.

[36] T. Ando, J. Phys. Soc. Jpn. **75**, 124701 (2006).

[37] P. Venezuela, M. Lazzeri, and F. Mauri, Phys. Rev. B **84**, 035433 (2011).

[38] J. Yan, Y. Zhang, P. Kim, and A. Pinczuk, Phys. Rev. Lett. **98**, 166802 (2007).

[39] C. Neumann, S. Reichardt, P. Venezuela, M. Drögeler, L. Banszerus, M. Schmitz, K. Watanabe, T. Taniguchi, F. Mauri, B. Beschoten, et al., Nat. Commun. **6**, 8429 (2015).

[40] D. M. Basko, S. Piscanec, and A. C. Ferrari, Phys. Rev. B **80**, 165413 (2009).

[41] M. Schütt, P. M. Ostrovsky, I. V. Gornyi, and A. D. Mirlin, Phys. Rev. B **83**, 155441 (2011).

[42] R. Vidano, D. Fischbach, L. Willis, and T. Loehr, Solid State Commun. **39**, 341 (1981).

[43] C. B. McKitterick, D. E. Prober, and M. J. Rooks, Phys. Rev. B **93**, 075410 (2016).

[44] A. Mogulkoc, M. Modarresi, B. Kandemir, M. Roknabadi, N. Shahtahmasebi, and M. Behdani, Physica B: Condensed Matter **446**, 85 (2014).

[45] S. Bae, H. Kim, Y. Lee, X. Xu, J.-S. Park, Y. Zheng, J. Balakrishnan, T. Lei, H. Ri Kim, Y. I. Song, et al., Nat. Nanotech. **5**, 574 (2010).

[46] X. Li, W. Cai, J. An, S. Kim, J. Nah, D. Yang, R. Piner, A. Velamakanni, I. Jung, E. Tutuc, et al., Science **324**, 1312 (2009).

[47] A. A. Lagatsky, Z. Sun, T. S. Kulmala, R. S. Sundaram, S. Milana, F. Torrisi, O. L. Antipov,

Y. Lee, J. H. Ahn, C. T. A. Brown, et al., Appl. Phys. Lett. **102**, 013113 (2013).

[48] L. G. Cançado, A. Jorio, E. H. M. Ferreira, F. Stavale, C. A. Achete, R. B. Capaz, M. V. O. Moutinho, A. Lombardo, T. S. Kulmala, and A. C. Ferrari, Nano Lett. **11**, 3190 (2011).

[49] A. Das, S. Pisana, B. Chakraborty, S. Piscanec, S. K. Saha, U. V. Waghmare, K. S. Novoselov, H. R. Krishnamurthy, A. K. Geim, A. C. Ferrari, et al., Nat. Nanotech. **3**, 210 (2008).

[50] M. Bruna, A. K. Ott, M. Ijäs, D. Yoon, U. Sassi, and A. C. Ferrari, ACS Nano **8**, 7432 (2014).

[51] F. Bonaccorso, A. Lombardo, T. Hasan, Z. Sun, L. Colombo, and A. C. Ferrari, Mater. Today **15**, 564 (2012).

[52] A. V. Baranov, A. N. Bekhterev, Y. S. Bobovich, and V. I. Petrov, Opt. Spectroscopy **62** (1987).

[53] C. Thomsen and S. Reich, Phys. Rev. Lett. **85**, 5214 (2000).

[54] P. Tan, L. An, L. Liu, Z. Guo, R. Czerw, D. L. Carroll, P. M. Ajayan, N. Zhang, and H. Guo, Phys. Rev. B **66**, 245410 (2002).

[55] L. G. Cançado, M. A. Pimenta, R. Saito, A. Jorio, L. O. Ladeira, A. Grueneis, A. G. Souza-Filho, G. Dresselhaus, and M. S. Dresselhaus, Phys. Rev. B **66**, 035415 (2002).

[56] M. Marangoni, D. Brida, M. Quintavalle, G. Cirmi, F. M. Pigozzo, C. Manzoni, F. Baronio, A. Capobianco, and G. Cerullo, Opt. Express **15**, 8884 (2007).

[57] R. R. Nair, P. Blake, A. N. Grigorenko, K. S. Novoselov, T. J. Booth, T. Stauber, N. M. R. Peres, and A. K. Geim, Science **320**, 1308 (2008).

[58] E. Pop, V. Varshney, and A. K. Roy, MRS Bull. **37**, 1273 (2012).

[59] S. de Gironcoli, Phys. Rev. B **51**, 6773 (1995).

[60] P. Giannozzi, S. Baroni, N. Bonini, M. Calandra, R. Car, C. Cavazzoni, D. Ceresoli, G. L. Chiarotti, M. Cococcioni, I. Dabo, et al., J. Phys. Condens. Matter **21**, 395502 (2009).

[61] Y. Wang, J. E. Panzik, B. Kiefer, and K. K. M. Lee, Sci. Rep. **2** (2012).

[62] C. Nef, L. Posa, P. Makk, W. Fu, A. Halbritter, C. Schonenberger, and M. Calame, Nanoscale **6**, 7249 (2014).